Effect of potential truncations and shifts on the solid-liquid phase coexistence of Lennard-Jones fluids

Alauddin Ahmed and Richard J. Sadus[a)]
Centre for Molecular Simulation, Swinburne University of Technology, P.O. Box 218, Hawthorn, Victoria 3122, Australia

(Received 17 June 2010; accepted 28 July 2010; published online 30 September 2010)

Molecular simulation results for the solid-liquid coexistence properties of untruncated, truncated, truncated and shifted, and truncated and shifted-force 12-6 Lennard-Jones potentials are reported. It is found that solid-liquid coexistence properties vary systematically with potential truncations, shifts, and cut-off values. Potential truncations and shifts have important consequences at low temperatures, particularly in the vicinity of the triple point. The main influence is on the coexistence pressure whereas both liquid and solid densities are less sensitive to the truncations and shifts. The data reported in this work indicate that the cut-off radius mainly affects the properties of the liquid phase whereas its influence on the solid phase is almost negligible. The data suggest a monotonic variation of the melting temperature as a function of cut-off radius, which contradicts the oscillatory behavior of the melting temperature reported elsewhere. © *2010 American Institute of Physics*. [doi:10.1063/1.3481102]

I. INTRODUCTION

The thermodynamic properties of fluids, phase transitions, rheological characteristics, and interfacial properties are just a few examples of the many properties that have been studied[1] successfully using different implementations of the 12-6 Lennard-Jones (LJ) potential. The different implementations of the LJ potentials can be categorized in terms of the truncations and shifting schemes used.[1–4] The most commonly used truncation is to assign a fixed cut-off radius and recover the contribution of the full potential via long-range corrections. The benefit of using such a truncation is a significant reduction of computation time. However, truncating the potential often introduces additional inaccuracies, particularly if phase coexistence properties are involved. For example, calculations using cut-off radii of $r_c > 2.5\sigma$ (where σ is the characteristic LJ distance parameter) result in up to a 2% fluctuation in melting temperatures.[5] A study[6] on the effect of the cut-off radius on thermodynamic properties using a continuation method[7] concluded that the normal long-range corrections are only exact near the triple point for $r_c \geq 4\sigma$. The vapor-liquid phase equilibria of the LJ potential with cut-off radii 2σ, 2.5σ, and 5σ showed that the details of the truncation significantly change the shape of the vapor-liquid phase diagram.[4,8,9]

An alternative to simple potential truncation is to use a shifted-force implementation of the LJ potential. The vapor-liquid phase diagram of the shifted-force[10,11] LJ potential and the critical points obtained for truncated, truncated-shifted, and long-range corrected LJ systems vary significantly with cut-off radius.[12] A similar variation is observed when the shifted force LJ potential is used[11] to estimate the triple point.

Most solid-liquid coexistence studies have considered only a single cut-off radius and applied long range corrections. Recently, Mastny and de Pablo[5] calculated the Gibbs free energy of both the solid and liquid phases using extended ensemble density-of-states Monte Carlo simulation.[13] They calculated the effect of cut-off radius on the melting temperature and concluded that the effect of the cut-off radius is more pronounced on the solid phase than on the liquid phase. We are not aware of any study that has compared the thermodynamic properties at solid-liquid coexistence using the truncated Lennard-Jones (tLJ), truncated and shifted Lennard-Jones (tsLJ), and truncated and shifted-force (sfLJ) potentials. Therefore, the effect of potential cut-off and shifts on the LJ solid-liquid phase equilibria has not been fully resolved.

The aim of this work is to determine the effect of different truncations and shifts on the solid-liquid coexistence properties of the LJ potential. We report solid-liquid coexistence data for the different schemes as a function of cut-off radius. In addition, results are reported for the full LJ potential from near the triple point up to very high pressures.

II. METHODS

A. Potential models

The potential models used in this work are obtained from the original untruncated version of the 12-6 LJ potential defined by

$$u(r) = 4\varepsilon\left\{\left(\frac{\sigma}{r}\right)^{12} - \left(\frac{\sigma}{r}\right)^{6}\right\}, \tag{1}$$

where r is the distance between two particles and ε is the characteristic energy parameter. The variants[1] of the LJ potential, based on different truncations and shifts, are detailed below.

[a)]Electronic mail: rsadus@swin.edu.au.

(i) tLJ potential:

$$u_{\mathrm{tLJ}}(r)=\begin{cases}u(r), & r\le r_c\\ 0, & r>r_{c,}\end{cases} \tag{2}$$

where r_c is the radial distance of the potential cut-off.

(ii) tsLJ potential:

$$u_{\mathrm{tsLJ}}(r)=\begin{cases}u(r)-u(r_c), & r\le r_c\\ 0, & r>r_c.\end{cases} \tag{3}$$

(iii) sfLJ potential:

$$u_{\mathrm{sfLJ}}(r)=\begin{cases}u(r)-u(r_c)-(r-r_c)\left(\dfrac{du}{dr}\right)_{r_c}, & r\le r_c\\ 0, & r>r_c.\end{cases} \tag{4}$$

B. GWTS simulations

1. Background

We have used the GWTS algorithm[14,15] that combines the techniques of both equilibrium molecular dynamics (EMD) and nonequilibrium molecular dynamics (NEMD) simulations. This method has been recently tested elsewhere.[16,17] The GWTS algorithm takes advantage of the fact that a system under shear approaches steady state much faster than the conventional EMD.

We assume that for a given temperature, a liquid density ρ_{liq} (freezing point) and a solid density ρ_{sol} (melting point) exists within a set of possible densities $\{\rho_1,\rho_2,\ldots,\rho_k\}$. As depicted in Fig. 1, the GWTS algorithm involves the following steps.

Step 1. For all the possible densities at a given temperature, run one EMD (i.e., $\dot{\gamma}_0=0$) simulation and two NEMD simulations for strain rates $\dot{\gamma}_1$ and $\dot{\gamma}_2$.

Step 2. From the results obtained from step 1, identify the first density at which a pressure jump is observed going from zero to nonzero strain rates. This is the freezing density. To identify the freezing density accurately, a density increment of 0.01 (in reduced units) is typically required.

Step 3. Generate a density-pressure isotherm from EMD simulations for the set of densities $\{\rho_1,\rho_2,\ldots,\rho_k\}$. This isotherm will not be continuous: there are two distinct curves for the liquid and solid phases.

Step 4. Identify the freezing density ρ_{liq} on the density-pressure isotherm.

Step 5. Draw a tie line from the freezing point to the other curve. The point of intersection is the melting point density ρ_{sol}.

A particular advantage of the GWTS algorithm is that it is self-starting, which allows us to obtain the initial (and other) coexistence point *a priori*. The initial configuration in all the simulations was a face centered cubic (fcc) lattice structure.

2. Simulation details

The isothermal isochoric NEMD simulations were performed by applying the standard *sllod* equations[18] of motion for planner Couette flow coupled with Lees–Edwards[1,18] periodic boundary conditions. If the applied strain rate is switched off in the *sllod* algorithm it behaves like Newton's equations of motion and NEMD converts to EMD. The NVT EMD simulations were performed by applying conventional cubic periodic boundary conditions.[1] In these molecular dynamics simulations a Gaussian thermostat multiplier[19] was used to keep the kinetic temperature of the fluid constant. The equations of motion were integrated with a five-value Gear predictor corrector scheme.[18,20] The normal convention was adopted for the reduced density ($\rho^*=\rho\sigma^3$), temperature ($T^*=kT/\varepsilon$), energy ($E^*=E/\varepsilon$), pressure ($p^*=p\sigma^3/\varepsilon$), and time ($\tau^*=[\varepsilon/m\sigma^2]^{1/2}\tau$). All quantities quoted in this work are in terms of these reduced quantities and the superscript asterisk will be omitted in the rest of the paper. All simulation trajectories were typically run for 2×10^5 time steps. The first 5×10^4 time steps of each trajectory were used either to equilibrate zero-shearing field equilibrium molecular dynamics or to achieve nonequilibrium steady state after the shearing field is switched on. The rest of the time steps in each trajectory were used to accumulate the average values of thermodynamic variables with average standard deviations. All the GWTS data presented in this work were averaged over 5–10 independent simulations. A system size of 4000 Lennard-Jones particles was used for the GWTS simulations.

To check that the GWTS algorithm gives the true equilibrium coexistence point, we estimated the Gibbs function using the equation of state of Johnston *et al.*[21] For example, at the solid-liquid coexistence point at $T=2.74$, the reduced Gibbs function for the liquid and solid phases was found to

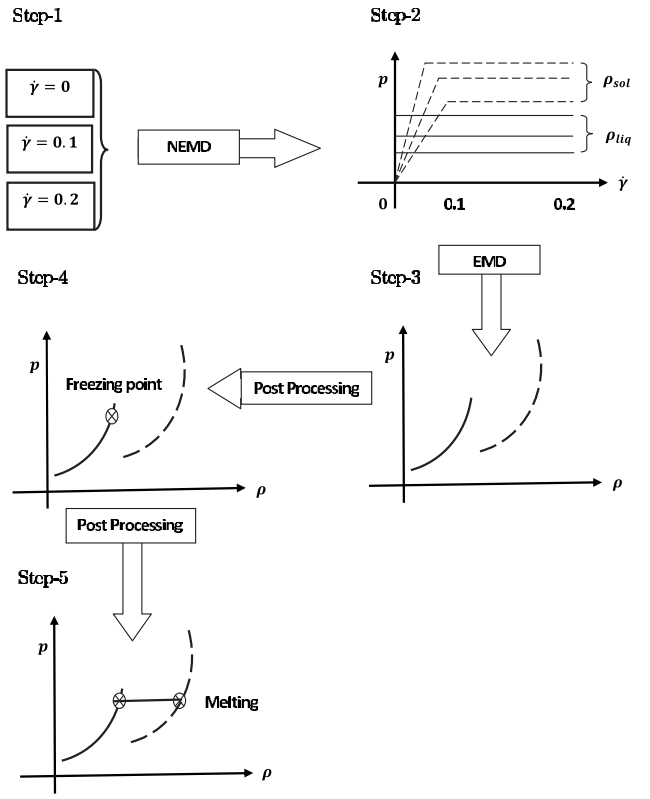

FIG. 1. Schematic illustration of the five steps involved in the GWTS algorithm. The liquid (——) and solid (- - -) phases are identified. See text for details.

be 35.69 and 35.60, respectively. The near equivalence of these values confirms that the phases are in equilibrium.

C. Gibbs–Duhem integration (GDI) simulations

1. Background

GDI simulations[22] involve the integration of the Clapeyron equation. For a one-component system, the Gibbs–Duhem equation is

$$d(\beta\mu) = hd\beta + \beta v dp, \tag{5}$$

where μ is the chemical potential, h is the molar enthalpy, v is the molar volume, and $\beta = 1/kT$. The Clapeyron equation is obtained by writing Eq. (5) for two coexisting phases (I and II)

$$\left(\frac{dp}{d\beta}\right)_s = -\frac{\Delta h}{\beta \Delta v}, \tag{6}$$

where $\Delta h = h_{\mathrm{I}} - h_{\mathrm{II}}$ and $\Delta v = v_{\mathrm{I}} - v_{\mathrm{II}}$ are the differences in the molar enthalpies and molar volumes, respectively, of the coexisting phases. The subscript s indicates that the derivative is taken along the saturation line. Alternatively

$$\left(\frac{d \ln p}{d\beta}\right)_s = -\frac{\Delta h}{\beta p \Delta v} = f(\beta, p). \tag{7}$$

Equations (6) and (7) regulate the change in pressure required to maintain two-phase coexistence. If the pressure at a given coexistence point is known either of these equations can be integrated numerically to obtain the entire coexistence curve. In practice, Eq. (7) is preferred to Eq. (6) because the right hand side of Eq. (6) varies only slowly. There are many different strategies[1] to solve differential equations. In this work, we implemented the Adams predictor-corrector algorithm as detailed elsewhere.[22]

2. Simulation details

Solid-liquid coexistence at different temperatures was determined using the GDI algorithm[22] with an initial starting point obtained from the GWTS algorithm described in the previous section. The Clapeyron equation used in the evaluation of the GDI series was shown to be related to the stability of the integration at a given temperature.[22] It has been demonstrated in Ref. 22 that for the LJ potential two different versions of Clapeyron equation must be used below [inverse of Eq. (7)] and above [Eq. (7)] the temperature of $T=2.74$ to maintain the stability of integration. Therefore, we have chosen this temperature as the starting point of our GDI simulations. At the beginning of the simulation 932 atoms were distributed between boxes representing solid and liquid phases. The liquid phase box contained 432 atoms while the solid phase box contained 500 atoms in the fcc lattice structure. The simulations were performed in cycles. A simulation period of 10 000 was used to accumulate the simulation averages followed by a period of 10 000 equilibration cycles. In the series of simulations toward $T>2.74$, the temperature change per step in the decreasing direction was $\Delta\beta=0.01$,

TABLE I. Solid-liquid coexistence properties of the full 12-6 LJ potential obtained in this work using the GDI algorithm starting with the coexistence properties obtained from the GWTS algorithm at $T=2.74$. The statistical uncertainty in the last digit is given in brackets.

T	p	ρ_{liq}	ρ_{sol}	T	p	ρ_{liq}	ρ_{sol}
66.666 67	2969(6)	2.040(3)	2.122(4)	3.508 77	51.6(2)	1.192(1)	1.259(1)
40	1520(4)	2.001(1)	2.113(8)	3.389 83	48.9(1)	1.184(1)	1.249(1)
28.571 43	974(1)	1.925(2)	2.008(3)	3.278 68	46.5(1)	1.174(1)	1.241(1)
22.222 22	698(1)	1.819(2)	1.900(1)	3.174 60	44.0(1)	1.166(2)	1.233(1)
18.181 82	534(1)	1.738(2)	1.813(2)	3.076 92	41.8(1)	1.158(2)	1.224(1)
15.384 62	426(1)	1.670(2)	1.744(1)	2.985 07	39.9(1)	1.151(2)	1.218(1)
13.333 33	352(1)	1.617(2)	1.690(1)	2.898 55	37.9(1)	1.144(3)	1.211(1)
11.764 71	297.1(5)	1.569(2)	1.643(1)	2.816 90	36.2(2)	1.136(2)	1.204(1)
10.526 32	255.6(5)	1.532(1)	1.601(2)	2.739 72	34.4(1)	1.127(1)	1.196(1)
9.523 81	222.4(3)	1.496(2)	1.564(1)	2.290(5)	28.0966	1.085(1)	1.149(1)
8.695 65	195.6(7)	1.462(2)	1.532(1)	2.065(5)	22.7861	1.065(1)	1.134(1)
8	174.4(3)	1.437(2)	1.504(1)	1.839(5)	18.4674	1.039(1)	1.108(1)
7.407 40	156.5(3)	1.409(1)	1.478(1)	1.651(5)	14.9276	1.016(1)	1.088(1)
6.896 55	141.6(4)	1.388(1)	1.456(1)	1.491(6)	12.0379	0.995(2)	1.068(1)
6.451 61	128.6(3)	1.367(2)	1.434(1)	1.354(6)	9.6725	0.975(1)	1.051(1)
6.060 60	117.8(4)	1.349(2)	1.416(1)	1.237(6)	7.7390	0.959(2)	1.036(1)
5.714 28	107.9(2)	1.330(2)	1.397(1)	1.138(7)	6.1600	0.942(2)	1.021(1)
5.405 40	99.4(2)	1.312(2)	1.379(1)	1.054(6)	4.8639	0.929(2)	1.011(1)
5.128 20	92.0(3)	1.298(2)	1.364(1)	0.983(7)	3.8048	0.915(1)	1.001(1)
4.878 04	85.5(2)	1.286(2)	1.350(1)	0.923(7)	2.9363	0.905(1)	0.994(1)
4.651 16	79.7(2)	1.270(1)	1.336(1)	0.873(7)	2.2296	0.893(2)	0.986(1)
4.444 44	74.4(3)	1.256(2)	1.323(1)	0.831(7)	1.6502	0.886(1)	0.979(1)
4.255 31	69.6(1)	1.246(2)	1.311(1)	0.795(7)	1.1748	0.877(2)	0.975(1)
4.081 63	65.3(1)	1.233(1)	1.299(1)	0.766(7)	0.7850	0.872(1)	0.971(1)
3.921 56	61.5(1)	1.222(1)	1.288(1)	0.741(7)	0.4673	0.866(2)	0.967(1)
3.773 58	58.0(2)	1.212(2)	1.278(1)	0.721(7)	0.2063	0.860(2)	0.965(1)
3.636 36	54.7(1)	1.203(1)	1.268(1)	0.704(7)	0.0069	0.858(2)	0.963(1)

where β is the reciprocal of the temperature. We have also tested three different series with different $\Delta\beta$ and found no difference in the results. For the simulation series toward $T<2.74$, the integration step size was $\ln p=-0.2$.

D. Calculation of properties for the full LJ potential

As the tLJ, tsLJ, and sfLJ potentials are benchmarked against the LJ potential, numerical values for the LJ potential are summarized in Table I. The 12-6 LJ potential was truncated at half of the box length and appropriate long-range correction terms[1] were evaluated to recover the contribution to pressure and energy of the full potential. The box lengths vary with density, i.e., $L=(N/\rho)^{1/3}$, which means that the cut-off distance (half the box length) is different at different densities. For example at $T=2.74$, the half box lengths for the freezing and melting densities were 7.65σ and 7.5σ, respectively. The long-range corrections were automatically updated to reflect this change in box length with density. The same procedure was adopted both for the GWTS and the GDI algorithms. The GDI calculations for the full LJ potential were initiated with the coexistence pressure and liquid and solid densities at a chosen temperature ($T=2.74$) obtained from full LJ calculations via the GWTS algorithm.

III. RESULTS AND DISCUSSION

The solid-liquid coexistence properties were examined at two different temperatures as the cut-off radius increased from 2.5σ to 6.5σ in steps of 0.5σ. Figure 2 shows the variation of pressure as a function of cut-off radius at $T=1$ [Fig. 2(a)] and $T=2.74$ [Fig. 2(b)]. In general, the pressure decreases systematically with the increase of cut-off radius. The tLJ and tsLJ potentials yield the same pressure because the shift is a constant value [see Eq. (3)], which does not affect the derivative used in calculating the virial contribution to pressure. In contrast, the sfLJ potential yields considerably higher values of pressure, particularly at small cut-off values. At all cut-off values, the differences in pressures between the different LJ potentials are less noticeable at $T=2.74$ than $T=1$, which reflects the greater relative contribution of kinetic interactions at the higher temperature.

We note that our results for the sfLJ potential with a cut-off radius $r_c=2.5\sigma$ are slightly different to GDI data reported by Errington *et al.*[11] Our coexistence pressure, liquid density, and solid density are 5.83%, 1.84%, and 1.56% lower, respectively, than their results. These discrepancies could be largely attributed to finite-size effects and errors in choosing the original reference point. We have validated our sfLJ data with results reported by Powles *et al.*[10] for a cut-off radius $r_c=3\sigma$ and obtained very good agreement.

The use of potential truncations and shifts requires the addition of long-range corrections to recover the full contribution to pressure. In contrast, Powles[23] did the exact opposite, i.e., the pressure was corrected from the full LJ pressure to that of the tsLJ and sfLJ pressure. This transformation mechanism was verified via the equation of state of Nicolas *et al.*[24] and simulations on truncated-shifted and sfLJ potentials. In the same spirit, Johnson *et al.*[21] rigorously derived mean-field corrections for the tsLJ potential and found remarkable accuracy for these corrections at $r_c=4\sigma$. However, they also found that the accuracy of the mean-field corrections was compromised for lower cut-off radii in the case of the tsLJ potential and could only produce reasonable results for $r_c>3\sigma$.

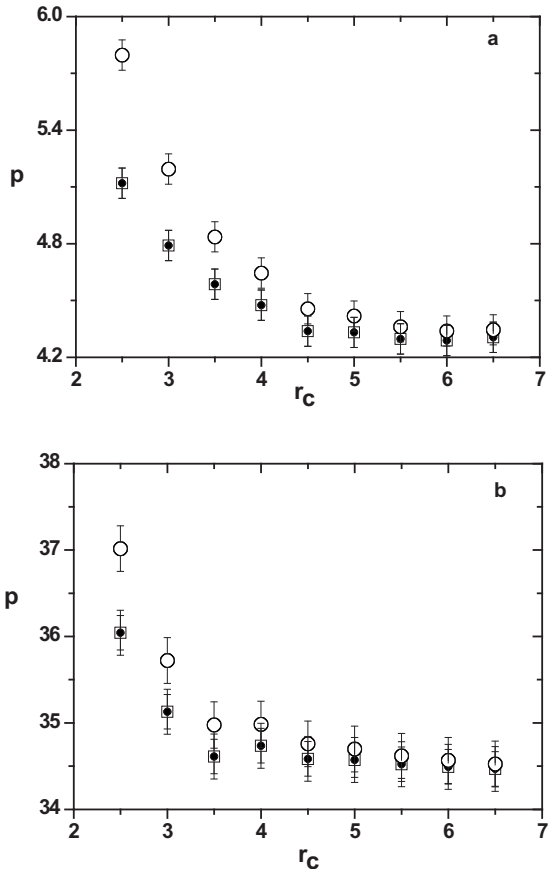

FIG. 2. Solid-liquid coexistence pressures of various 12-6 LJ potentials as a function of cut-off radius (relative to σ). Results are shown for the tLJ (□), tsLJ (●), and sfLJ (○) potentials at temperatures of (a) $T=1.0$ and (b) $T=2.74$.

The configurational energy variation with respect to cut-off values is shown in Figs. 3 and 4. In common with the pressure results, Figs. 3 and 4 show that the configurational energy at solid-liquid coexistence depends both on the cut-off radius and on the shift used. The energy variation is more prominent for the lower cut-off values. At $T=1$ and at $r_c=2.5\sigma$, the tsLJ and sfLJ potentials yield energies that are 9.34% and 21% higher, respectively, than those observed for the tLJ potential. This gap becomes progressively smaller at higher cut-off values.

In contrast to the results for the liquid phase (Fig. 3), the tLJ configurational energies obtained for the solid phase (Fig. 4) are relatively insensitive to the cut-off values. This result is also in contrast to the solid phase energies obtained for the tsLJ and sfLJ potentials, which are both dependent on the cut-off radius, particularly at low values.

We found that, at any given temperature, the liquid and solid phase coexisting densities only vary by approximately $10^{-2}-10^{-3}$ depending on the truncations and shifts used. This is in contrast to the significant potential dependencies observed in the densities for vapor-liquid phase equilibria at

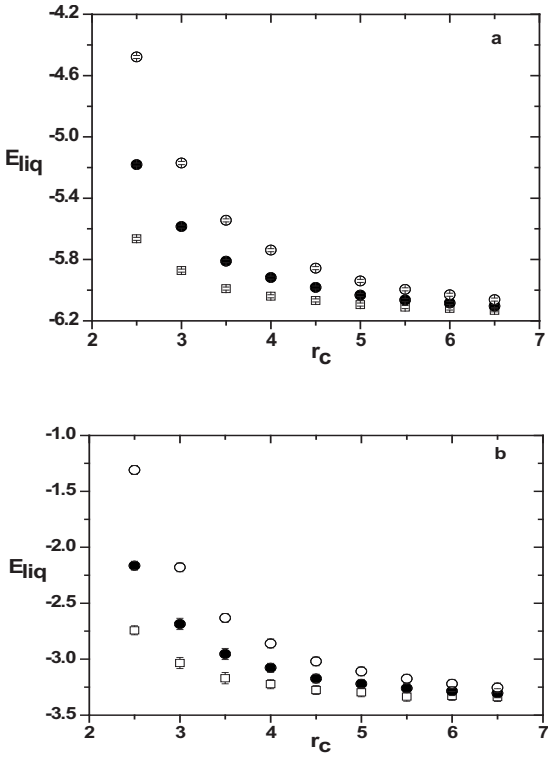

FIG. 3. Configurational energy of the coexisting liquid phase for various 12-6 LJ potentials as a function of cut-off radius (relative to σ). Results are shown for the tLJ (□), tsLJ (●), and sfLJ (○) potentials at temperatures of (a) $T=1.0$ and (b) $T=2.74$.

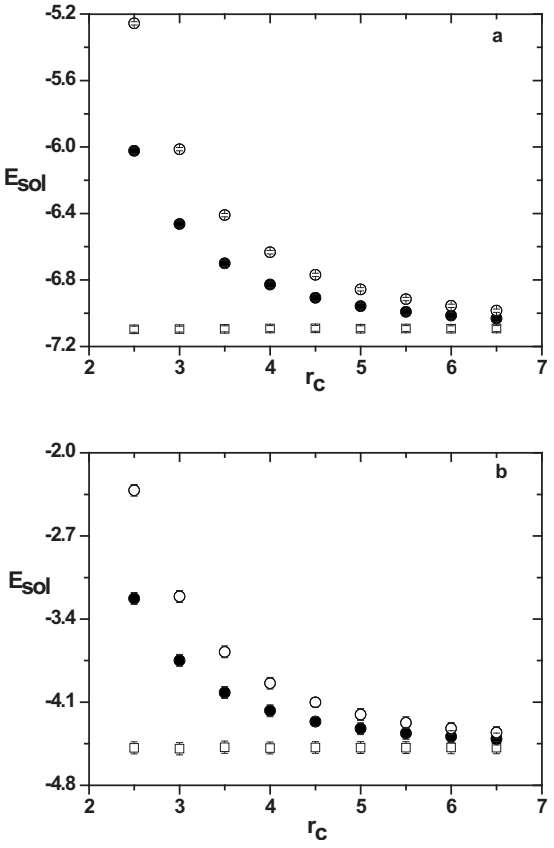

FIG. 4. Configurational energy of the coexisting solid phase for various 12-6 LJ potentials as a function of cut-off radius (relative to σ). Results are shown for the tLJ (□), tsLJ (●), and sfLJ (○) potentials at temperatures of (a) $T=1.0$ and (b) $T=2.74$.

different temperatures. At low temperatures ($T=1.0$) the density of the liquid phase varies by ± 0.002 depending on the cut-off radius. In contrast, at higher temperatures ($T=2.74$) there is no noticeable dependency on the cut-off radius. The solid phase densities are almost insensitive to the cut-off value irrespective of the temperature. This observation is in contrast to the work of Mastny and de Pablo,[5] which reported that solid phase densities were more dependent on the cut-off radius than liquid phase densities.

Since the melting temperature and pressure are related through the Clausius–Clapeyron equation, a small change in temperature affects the pressure and vice versa. As our data suggest a monotonic variation of pressure with respect to cut-off distance, we can also expect a monotonic change of melting temperature as a function of cut-off radius. In contrast to this observation, Mastny and de Pablo[5] found an oscillatory behavior of melting temperature with increasing cut-off values. No theoretical justification was provided for such aberrant behavior. In view of the fact that vapor-liquid equilibria pressure and temperature also vary regularly as a function of cut-off radius, Mastny and de Pablo's[5] observation may be an artifact of the simulation algorithm. In common with the well-known system-size dependency of melting line properties, the effect of cut-off radius may be algorithm dependent.

Figures 5(a) and 5(b) compare solid-liquid coexistence pressures for the tsLJ, sfLJ, (both at a cut-off radius of 2.5σ), and the full LJ potentials. It is apparent from this comparison that the tsLJ and sfLJ yield similar deviations from the LJ

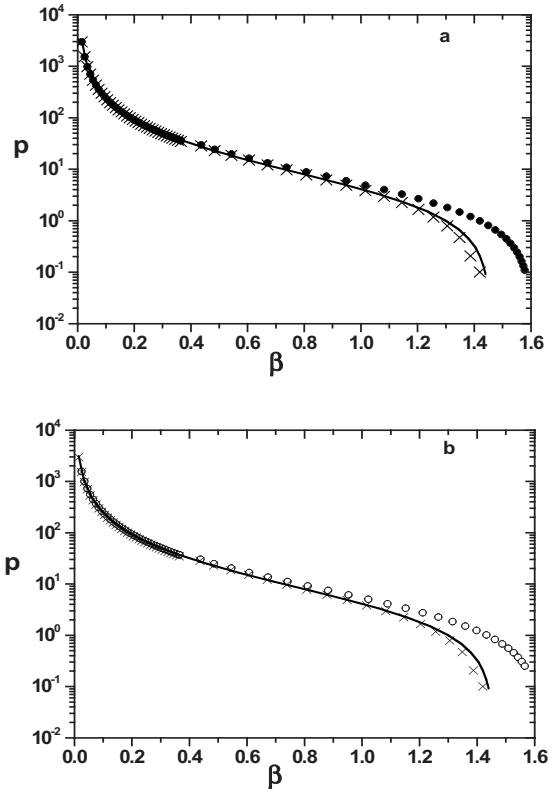

FIG. 5. Comparison of the solid-liquid coexistence pressure obtained from (a) tsLJ (●) and (b) sfLJ (○) at a cut-off radius of 2.5σ. In both cases a comparison is made with the full LJ potential obtained in this work (×) and reported by Agrawal and Kofke (—, Ref. 22).

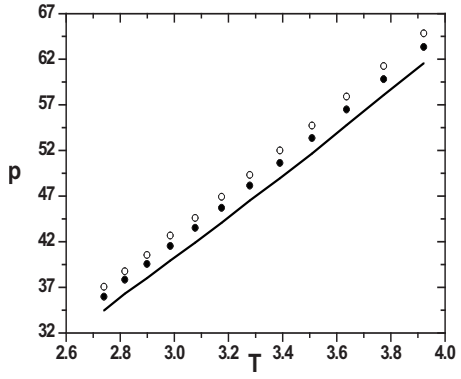

FIG. 6. Comparison of the solid-liquid coexistence pressure and temperature obtained from the sfLJ (○) and tLJ (●) potentials. The melting line pressure for the full LJ (—) potential, obtained in this work, is also given for comparison.

potential as a function of temperature. Indeed, for either the tsLJ or sfLJ, deviations from the LJ pressure only become really significant at very low temperatures, i.e., in the proximity of the triple point. It is apparent that both the tsLJ and sfLJ potentials would predict a lower triple point temperature than the LJ potential.

The pressures obtained from the sfLJ and tLJ potentials at a common cut-off radius ($r_c=2.5\sigma$) are compared to the full LJ potential in Fig. 6. It is apparent from this comparison that either truncating or shifting the potential considerably increases the coexistence pressure. In particular, the sfLJ calculations yield significant deviations from the full LJ pressure.

Figure 7 illustrates the effect of the cut-off radius on the melting pressure obtained at different temperatures using the tsLJ potential. The comparison with results obtained from the full LJ potential indicates that choosing a small cut-off value ($r_c=2.5\sigma$) consistently results in an increase in the melting pressure at all temperatures. A significantly higher cut-off value ($r_c=6.5\sigma$) yields good agreement with the LJ potential at low temperatures but the pressures are slightly under predicted at $T>3.2$.

Figure 8 illustrates the effect of the cut-off radius on the temperature-density behavior of the sfLJ potential. When a small cut-off value is used ($r_c=2.5\sigma$) both the coexisting

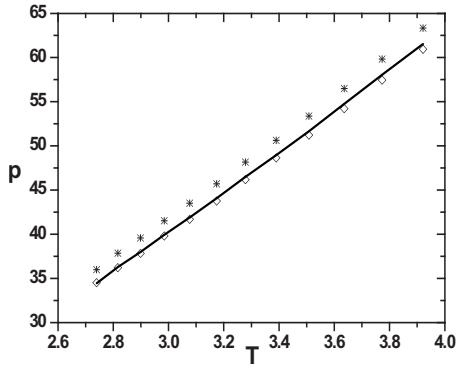

FIG. 7. The solid-liquid coexistence pressure and temperature of the tsLJ potential at different cut-off values. Shown are cut-off values of 2.5σ (*) and 6.5σ (◇). The melting line pressure for the full LJ (—) potential, calculated in this work, is also given for comparison.

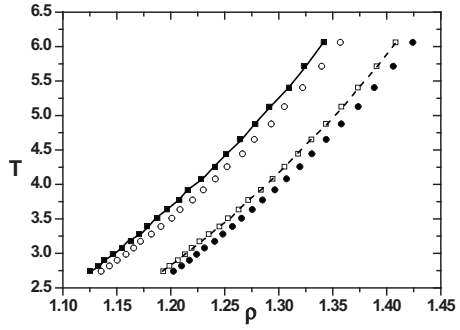

FIG. 8. Temperature-density behavior of sfLJ potential. Shown are the freezing (■) and melting (□) lines with a cut-off radius of 6.5σ and freezing (○) and melting (●) lines with a cut-off radius of 2.5σ. A comparison is shown with the full LJ freezing line (—) and melting line (---) obtained in this work.

liquid and solid phase densities are increased at all temperatures. In contrast a cut-off value of $r_c=6.5\sigma$ results in densities that are almost indistinguishable from the LJ potential.

IV. CONCLUSIONS

The dependence of the solid-liquid coexistence properties for the truncated, truncated and shifted, and truncated shifted-force potentials is reported using the GWTS and GDI algorithms. It is found that solid-liquid coexistence properties vary systematically with potential truncations, shifts, and cut-off radius. A cut-off radius of 6.5σ is recommended to achieve consistency between all methods. Potential truncations and shifts have important consequences at low temperatures, particularly in the vicinity of the triple point. The main influence is on the coexistence pressure whereas both liquid and solid densities are less sensitive to truncations and shifts. In contrast to Mastny and de Pablo's[5] observation, the data reported in this work indicate that the cut-off radius mainly affects the properties of the liquid phase whereas its influence on the solid phase is almost negligible. The data suggest a monotonic variation of the melting temperature as a function of cut-off radius, which contradicts the oscillatory behavior of the melting temperature reported by Mastny and de Pablo.[5]

ACKNOWLEDGMENTS

We thank the Australian Partnership for Advanced Computing (APAC) for a generous allocation of computing time. One of the authors (A.A.) thanks Swinburne University of Technology for a postgraduate scholarship.

[1] R. J. Sadus, *Molecular Simulation of Fluids: Theory, Algorithms, and Object Orientation* (Elsevier, Amsterdam, 1999).
[2] M. P. Allen and D. J. Tildesley, *Computer Simulation of Liquids* (Clarendon, Oxford, 1987).
[3] D. Frenkel and B. Smit, *Understanding Molecular Simulation* (Academic, San Diego, 2001).
[4] B. Smit, J. Chem. Phys. **96**, 8639 (1992).
[5] E. A. Mastny and J. J. de Pablo, J. Chem. Phys. **127**, 104504 (2007).
[6] R. Vogelsang and C. Hoheisel, Mol. Phys. **55**, 1339 (1985).
[7] R. J. Baxter, J. Chem. Phys. **52**, 4559 (1970).
[8] A. Z. Panagiotopoulos, Int. J. Thermophys. **15**, 1057 (1994).
[9] J. E. Finn and P. A. Monson, Phys. Rev. A **39**, 6402 (1989); Phys. Rev. A **42**, 2458 (1990).
[10] J. G. Powles, W. A. B. Evans, and N. Quirke, Mol. Phys. **46**, 1347

(1982).
[11] J. R. Errington, P. G. Debenedetti, and S. Torquato, J. Chem. Phys. **118**, 2256 (2003).
[12] W. Shi and J. K. Johnson, Fluid Phase Equilib. **187–188**, 171 (2001).
[13] E. B. Kim, R. Faller, Q. Yan, N. L. Abbott, and J. J. de Pablo, J. Chem. Phys. **117**, 7781 (2002).
[14] J. Ge, G.-W. Wu, B. D. Todd, and R. J. Sadus, J. Chem. Phys. **119**, 11017 (2003).
[15] P. Mausbach, A. Ahmed, and R. J. Sadus, J. Chem. Phys. **131**, 184507 (2009).
[16] A. Ahmed and R. J. Sadus, J. Chem. Phys. **131**, 174504 (2009).
[17] A. Ahmed and R. J. Sadus, Phys. Rev. E **80**, 061101 (2009).
[18] D. J. Evans and G. P. Morriss, *Statistical Mechanics of Nonequilibrium Liquids*, 2nd ed. (Academic, London, 2008).
[19] D. J. Evans, W. G. Hoover, B. H. Failor, B. Moran, and A. J. C. Ladd, Phys. Rev. A **28**, 1016 (1983).
[20] A. W. Gear, *Numerical Initial Value Problems in Ordinary Differential Equations* (Prentice-Hall, Englewood Cliffs, 1971).
[21] J. K. Johnson, J. A. Zollweg, and K. E. Gubbins, Mol. Phys. **78**, 591 (1993).
[22] D. A. Kofke, J. Chem. Phys. **98**, 4149 (1993); R. Agrawal and D. A. Kofke, Mol. Phys. **85**, 43 (1995).
[23] J. G. Powles, Physica **126A**, 289 (1984).
[24] J. J. Nicolas, K. E. Gubbins, W. B. Street, and D. J. Tildesley, Mol. Phys. **37**, 1429 (1979).